Direct-drive high-convergence-ratio implosion studies on the OMEGA laser system*

F. J. Marshall,[†,a)] J. A. Delettrez, R. Epstein, V. Yu. Glebov, D. R. Harding, P. W. McKenty, D. D. Meyerhofer, P. B. Radha, W. Seka, S. Skupsky, V. A. Smalyuk, J. M. Soures, C. Stoeckl, R. P. J. Town, and B. Yaakobi
Laboratory For Laser Energetics, University of Rochester, 250 East River Road, Rochester, New York 14623-1299

C. K. Li, F. H. Séguin, D. G. Hicks, and R. D. Petrasso
Plasma Science And Fusion Center, Massachusetts Institute of Technology, 175 Albany St., Cambridge, Massachusetts 02139

(Received 18 November 1999; accepted 2 February 2000)

A series of direct-drive implosion experiments, using room-temperature, gas-filled CH targets, are performed on the University of Rochester's OMEGA laser system [T. R. Boehly *et al.*, Opt. Commun. **133**, 495 (1997)]. The target performance at stagnation and its dependence on beam smoothing and pulse shaping is investigated. Compressed core conditions are diagnosed using x-ray and neutron spectroscopy, and x-ray imaging. The individual beams of OMEGA are smoothed by spectral dispersion in two dimensions (2D SSD) with laser bandwidths up to ~0.3 THz, with 1 ns square to 2.5 ns shaped pulses. A clear dependence of target performance on pulse shape and beam smoothing is seen, with the target performance (yield, areal density, and shell integrity) improving as SSD bandwidth is applied. [S1070-664X(00)95405-3]

I. INTRODUCTION

Direct-drive, inertial confinement laser-driven fusion (ICF) is accomplished by near-uniform illumination of spherical fuel-bearing targets with high-power laser beams.[1–3] Ablation of the outer target material drives an implosion resulting in a large increase in temperature and density of the final fuel region. If sufficiently high fuel temperature (>10 keV) and surrounding areal density (>0.3 g/cm^2) are achieved,[2] then ignition, thermonuclear burn propagation, and gain can occur. Attaining near-ignition-scale conditions in direct-drive implosions requires controlling the growth of the Rayleigh–Taylor (RT) instability, seeded primarily by illumination nonuniformities and target imperfections. Direct-drive ignition designs for the National Ignition Facility (NIF), currently under construction,[4,5] consists of an ~1 μm thick, ~3 mm diam CH (plastic) shell surrounding an ~300 μm thick deuterium–tritium (DT) ice layer. There is a small residual DT gas (equivalent to ~3 atm at room temperature) in the target center from an ice layer near the triple point (19 K). Cryogenic targets planned for OMEGA are energy-scaled versions of NIF cryogenic targets with ~1 mm diam and ~90 μm ice thickness.

Room-temperature-target (noncryogenic) implosions are currently performed on the University of Rochester's OMEGA laser system,[6] which delivers up to ~30 kJ of 351 nm laser light in 1–3 ns. The targets consist of 20–40 μm thick plastic shells filled with up to 15 atm of various gases. These targets have a similar total mass to the OMEGA cryogenic targets and when irradiated with a 1 ns square pulse, have stability characteristics similar to cryogenic targets illuminated with a shaped pulse.[7] Previously reported OMEGA direct-drive implosion experiments have demonstrated the ability to achieve high temperatures[8] ($kT_e \sim 3$ to 4 keV, $kT_i \sim 14$ keV), attaining DT neutron yields of $>10^{14}$. The acceleration- and deceleration-phase target stability has been studied in spherical implosions using thin polymer layers doped with various high-Z elements (Ti, Cl, and Si), and D_2 fills containing a small Ar component.[9] The stagnation phase (maximum density and temperature conditions) of the implosions has been studied using both x-ray and neutron spectroscopic techniques concentrating on empty, hollow-shell targets or those with low-pressure (3 atm) gas fills.[10,11] The ability to achieve final CH areal densities in excess of ~100 mg/cm^2 was demonstrated. Additional experiments that incorporated Ti-doped layers within the shell have provided independent confirmation of the core conditions.[12,13]

The compressed target in these experiments can be separated into three regions at stagnation: Gas fill, inner (hot) shell, and outer (cold) shell. The performance of all regions is a function of the pulse shape, shell thickness, and single-beam uniformity. For high-shock-strength (1 ns square) pulses, the outer region shows the most sensitivity to single-beam uniformity, while for lower-shock-strength shaped pulses all regions show sensitivity to the single-beam uniformity. In this paper the sensitivity of all three regions to pulse shape, shell thickness, and single-beam uniformity is presented.

II. EXPERIMENTS

The targets used for these experiments consisted of 20–40 μm thick spherical shells ~950 μm in diameter. The shell material was either deuterated plastic (CD) with an un-

*Paper SI 1 1 Bull. Am. Phys. Soc. **44**, 282 (1999).
[†]Invited speaker.
[a)]Electronic mail: fredm@lle.rochester.edu

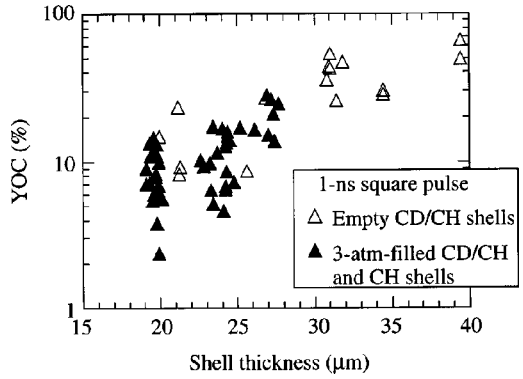

FIG. 1. Ratio of measured D–D neutron yield to calculated yield (YOC) for targets imploded with 1 ns square pulses; included are all targets with 3 atm fills (D_2, H_2, and DHe^3) and targets with and without CD inner layers. The yield from targets with H_2 fills comes solely from inner CD layers. Plotted for comparison are empty CD–CH-shell target results.

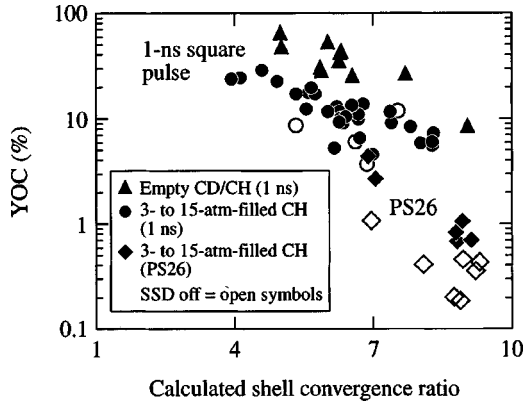

FIG. 2. YOC from 3–15 atm filled CH targets, for 1 ns square and PS26 pulse shapes, with and without SSD bandwidth (>0.2 THz) applied. The results from empty CD–CH shells imploded with 1 ns square pulses are shown for comparison.

deuterated plastic (CH) overcoat, or pure CH. All of the present experiments were performed on gas-filled shells, filled with 3–15 atm of H_2, D_2, and/or DHe^3. All targets were overcoated with a 0.1 μm Al gas retention barrier. (The DHe^3-filled targets had an equimolar mixture of D and He^3). The targets filled with H_2 allowed for measurement of the primary (D–D) and secondary (D–T) neutron yield from the CD layer, while the D_2- and DHe^3-filled targets allowed for measurement of the primary yield from the gas-fill region and the secondary yield from the gas-fill and shell-material regions. A parallel series of target experiments replaced the inner CD layer with a Ti-doped (4%–6% atomic fraction) CH layer. Emission from the Ti-doped region acts as a tracer of the doped-shell region, allowing for imaging of its shape and determination of its size. The experiments were performed using two pulse shapes: a 1 ns square pulse, and a 2.5 ns shaped pulse with a 1:8 foot-to-main-pulse aspect ratio (PS26, see details in Refs. 10 and 11). The OMEGA beams were phase converted using distributed phase plates[14] (DPP's) and smoothed by smoothing by spectral dispersion in two dimensions[15] (2D SSD) with either 3 by 3 or 3 by 10 GHz-frequency oscillators.

III. RESULTS

A. Gas-fill performance

Comparison of the measured primary fusion yield (D–D) to the yield calculated by the 1D hydrodynamics code LILAC[16] gives an overall measure of the performance of the target. Figure 1 shows the ratios of the measured to calculated yields [yield over calculated (YOC)] as a function of shell thickness for a series of 3 atm D_2-filled targets imploded with 1 ns square pulses ($\sim$27 kJ). The values obtained for targets with no gas fill (yield solely from the inner CD shell) are shown as open triangles. As was seen previously,[10] the highest YOC is obtained for the thickest targets, approaching unity for thicknesses of $\sim$40 μm. Where overlap exists, the gas-filled targets appear to follow this general trend, suggestive of a relation between shell thickness and performance.

Traditionally, target performance in ICF has been measured against the gas convergence ratio [initial gas outer radius/final gas outer radius (CR_{gas})]. The calculated CR_{gas} ranged from $\sim$20 to 50 for these experiments. Targets with the same calculated CR_{gas} but driven with different pulse shapes can have YOCs which vary by almost two orders of magnitude.[17] The target performance is much more sensitive to the shell thickness (Fig. 1). This suggests that the degree of nonuniformity in the shell, due to the growth of the RT instability, determines the overall target performance. To understand the effect of shell thickness and pulse shape on target performance, we have defined the calculated shell convergence ratio (CR_{shell}). This definition can also be used for shells with no gas fill. Applied to the empty-shell target case the ice-block final shell radius is given by

$$R_{\text{ice block}}=[3M_f/4\pi(\rho R)]^{1/2},$$

where M_f is the unablated shell mass and $(\rho R)_f$ is the shell areal density calculated at peak compression, where the values are calculated for the unablated shell material. The shell convergence ratio can then be defined as

$$CR_{\text{shell}}=R_i/R_f=R_i/R_{\text{ice block}}=R_i/[3M_f/4\pi(\rho R)]^{1/2},$$

where R_i is the initial shell radius. The YOC values as a function of CR_{shell} for both empty and gas-filled targets are plotted in Fig. 2. To accentuate the differences and minimize scatter, the cases in Fig. 2 are limited to low beam-energy variation [<10% beam-to-beam (rms) root-mean square]; the gas-filled targets additionally contain no CD in the shell, making them cases solely of gas-fill yield. The normalized yields for empty-shell targets have shown little discernible sensitivity to beam smoothing[10,11] (and are not separately identified), while the gas-filled targets show a difference for the extreme cases shown (no beam smoothing and $\Delta\upsilon_{\text{SSD}}\geqslant 0.2$ THz). The targets expected to have the lowest stability (PS26 pulse shape) show the most difference with and without SSD smoothing but also have the lowest values of YOC. The good correlation of YOC with CR_{shell} suggests that the shell integrity during compression dominates target

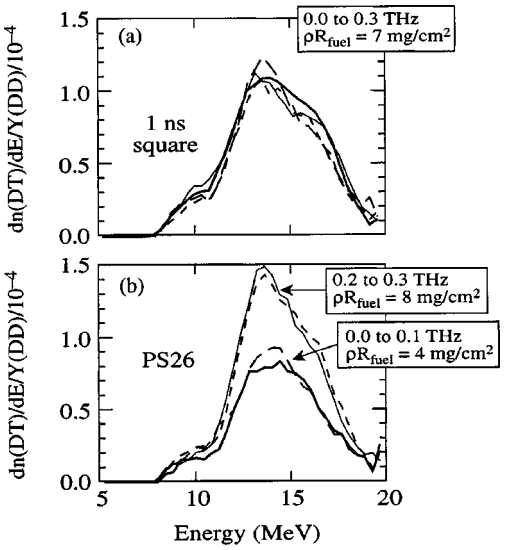

FIG. 3. SSD bandwidth dependence of the measured secondary (D–T) neutron spectra [normalized to the primary (D–D) neutron yield] from (a) 1 ns square and (b) PS26 pulse implosions.

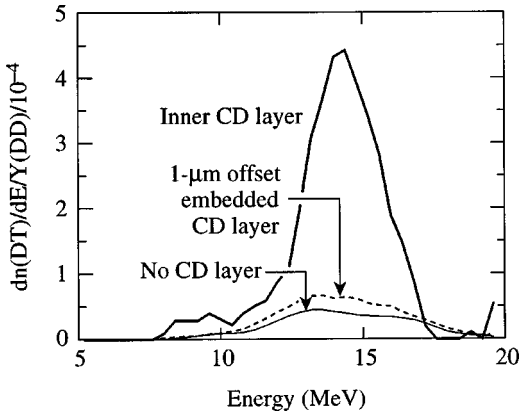

FIG. 4. The measured secondary neutron spectral shape from 27 μm thick, 3 atm filled CH shells with and without CD layers.

performance, including that of the gas fill. As was previously shown,[10,11] the shell performance is also noticeably affected by the presence of the gas fill.

The gas-fill performance is further characterized by measuring the fuel areal density ρR_{fuel}. Figure 3 shows measurements of the shape of the secondary neutron (D–T) spectra [$Y(DT) \propto \rho R_{\text{fuel}}$], using MEDUSA.[18] The targets are 3 atm-D_2-filled, 20 μm thick CH shells irradiated with 1 ns square pulses [Fig. 3(a)] and PS26 pulses [Fig. 3(b)] and various SSD bandwidths ($\Delta \nu_{\text{SSD}}$). The spectra from the 1 ns square pulse experiments show no discernible differences. Both the amplitude and the shape of the spectra are unchanged, which indicates that the average ρR_{fuel} is unchanged. Conversely, there is a very noticeable increase in the normalized secondary yield for the PS26 experiments versus $\Delta \nu_{\text{SSD}}$. Both the 0.2- and 0.3-THz cases are $\sim 2\times$ higher than the 0.0- and 0.1-THz cases. The ρR_{fuel} is deduced from a central source model, assuming no slowing down in the fuel, and as such, provides a lower limit on the value.[10,11] The statistical errors in the inferred values of ρR_{fuel} are typically 10%, due to the errors in the yield measurements. There is an additional systematic uncertainty of $\sim$25% due to the calibration uncertainty of the secondary yield detector. For 1 ns square pulses, the ρR_{fuel} values predicted by 1D simulations range from 21 to 23 mg/cm^2, while for PS26 they range from 73 to 78 mg/cm^2, where the variations in the simulations are due to variations in conditions (e.g., target thickness, energy of laser).

Figures 1–3 have shown the performance of the compressed gas fill as a function of pulse shape, single-beam uniformity, and shell thickness. Taken together, they show that (a) thicker shells give better performance compared to 1D simulations, and (b) the effect of single-beam nonuniformity on the performance is more apparent for more slowly rising pulse shapes. These results suggest that the shell integrity dominates the target performance. The differences in performance may be due to the lower isentropes obtained for the shaped-pulse implosions, resulting in smaller in-flight shell thicknesses and larger RT growth rates. This makes the targets more susceptible to breakup due to ablation-surface nonuniformities and to feedthrough of the nonuniformities to the inner surface. This conjecture is supported by simulations of imprint, RT growth, and saturation of the laser-induced nonuniformities.[7] The simulations show that for the most unstable targets (PS26 and thinner shells), the RT amplitude completely penetrates the shell during the acceleration phase. The characteristics of the shell, both the inner (hot) and outer (cold) regions, are discussed in the next two sections.

B. Inner (hot) shell performance

The state of the inner shell material is probed by tritons from the D–D reaction in the fill gas undergoing secondary reactions in the CD shell material. The normalized secondary neutron yields from 3 atm D_2 filled CH shells without a CD layer, with a 1 μm thick CD layer at the inner shell surface, or with an embedded 1 μm thick CD layer (offset 1 μm from the inner shell surface) are shown in Fig. 4. The targets were imploded with 1 ns square pulses. The inner CD layers have secondary yields that are much higher than the gas-only (no CD) case. The spectrum is also narrower, indicating significant slowing down of the tritons in the CD layer. The spectrum of the offset layer is almost equal to the gas-only case, indicating little if any significant mixing of the inner 2 μm region of the original shell at stagnation.

The results of the secondary yield contribution from the shell are shown in Fig. 5. The lower-limits of $\rho \Delta R_{\text{hot shell}}$ (of the CD layer) are calculated as described in Refs. 10 and 11, after adjustment for the contribution of the gas. For comparison, $\rho \Delta R$ values obtained from implosions of empty CD–CH targets and corresponding values for the CD layers from LILAC simulations are also shown. The measured $\rho \Delta R_{\text{hot shell}}$ values are near the limits predicted by LILAC indicating near 1D performance of the inner part of the compressed shell (probed by the D–D primary triton).

The inner (hot) shell is further investigated by imaging the x-ray emission from high-Z-doped target implosions. Figure 6 shows x-ray images from a series of target implosions with 2 μm thick, Ti-doped (4% atomic fraction) re-

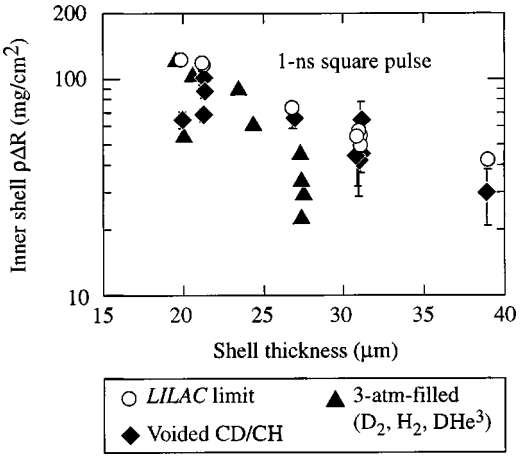

FIG. 5. $\rho\Delta R_{\text{hot shell}}$ lower-limit values for CD-bearing targets determined from the secondary (D–T) to primary (D–D) neutron yield ratio, along with LILAC predictions of the measurement limit. Empty CD–CH target values are shown for comparison.

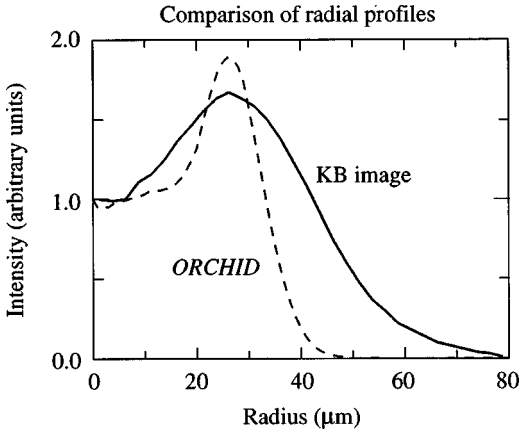

FIG. 7. Radial intensity profile of the high-bandwidth (0.3 THz) Ti-doped image and a 2D ORCHID simulation of the same. Both are norrnalized to 1.0 at the center.

gions, offset 1 μm from the inner shell surface. The SSD bandwidth was varied from 0.1 to 0.3 THz. The x-ray images were obtained with a Kirkpatrick–Baez (KB) microscope filtered to be sensitive from ~5 to 7 keV. The images clearly show a dependence on SSD bandwidth. The azimuthally averaged radial profiles of the images show a larger dip at the center (indicative of a thinner emitting region) for the high-bandwidth case. Figure 7 shows a comparison of the emission profile from the high-bandwidth (0.3 THz) SSD case with 2D ORCHID simulations. (ORCHID hydrodynamics simulations[19] modeled the single-beam nonuniformities including DPP contributions and SSD at 0.2 THz, assuming perfect beam balance, and no radiation.) The two profiles are seen to peak at approximately the same radius (27 μm), although the measured profile is wider than the simulated one. (Asymmetries, likely due to beam-to-beam energy variations, are contributing to this spread.)

The performance of the inner (hot) shell region shows dependence on pulse shape, shell thickness, and SSD bandwidth. The shell appears to be more compressed and integral with higher SSD bandwidth as seen in the limb-brightened images. The limit on $\rho\Delta R_{\text{hot shell}}$ deduced from the secondary yield is close to the LILAC predictions. Results from targets with offset CD layers indicate that there is little mixing over the initial inner 2 μm of the shell material, suggesting that the hot inner shell region is nearly intact at stagnation.

C. Outer (cold) shell performance

The cold-shell areal density ($\rho\Delta R_{\text{cold shell}}$) can be determined from the observed absorption in the continuum spectra obtained with a grating-dispersed KB microscope.[20] Figure 8 shows $\rho\Delta R_{\text{cold shell}}$ values from a series of 1 ns square pulse target experiments with varying shell thicknesses, with and without SSD beam smoothing. The values of $\rho\Delta R_{\text{cold shell}}$ are plotted as a function of shell thickness. [Both cases show the expected dependence on shell thickness as more cold shell material is left to absorb x-rays at stagnation.] The $\rho\Delta R_{\text{cold shell}}$ values obtained with SSD are substantially higher than those without. The values of $\rho\Delta R_{\text{cold shell}}$ from both 1D and 2D ORCHID simulations (solid symbols) show a similar trend as a function of shell thickness. The values of $\rho\Delta R_{\text{cold shell}}$ from ORCHID simulations were determined by a postprocessor which determined the $\rho\Delta R$ of the

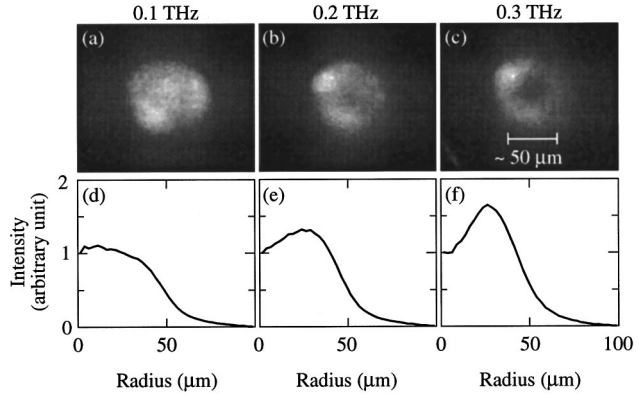

FIG. 6. Time-integrated, hard x-ray images (~5–7 keV) from a series of implosions of CH targets with inner Ti-doped layers for varying bandwidth [(a) 0.1, (b) 0.2, and (c) 0.3 THz], along with azimuthally averaged radial profiles of the same [(d)–(f)].

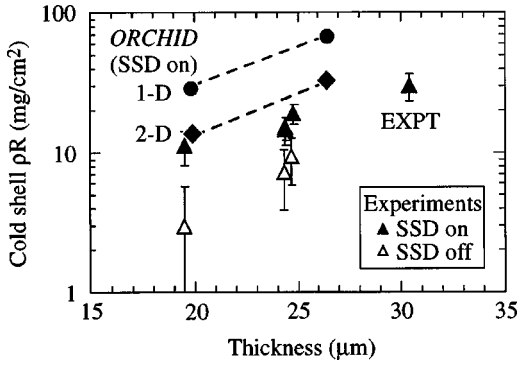

FIG. 8. Values of $\rho\Delta R_{\text{cold shell}}$ determined from grating dispersed KB microscope obtained x-ray spectra of 3 atm filled CH and CD–CH targets versus shell thickness, with (>0.2 THz) and without SSD bandwidth. The values obtained from 1D and 2D ORCHID simulations are shown for comparison.

unstripped fraction of the shell material from the density and temperature values as a function of position. The assumption is that this average value of $\rho\Delta R_{\text{cold shell}}$ is approximately directly measurable. (This is equivalent to a small optical depth approximation.) A more exact treatment would include radiation transport effects. In the 2D simulations the $\rho\Delta R_{\text{cold shell}}$ values are averaged over the radius of the emitting region. The 2D ORCHID predictions lie well below the 1D ORCHID predictions. Most of this reduction is due to the additional stripping of carbon ions in the disrupted shell material. Some is due to spatial modulation. The magnitude of the effects of single-beam nonuniformities appear to account for the observed lower value of $\rho\Delta R_{\text{cold shell}}$ from that expected by 1D simulations. (The single-beam nonuniformities in the 2D simulations affect the value of the simulated $\rho\Delta R_{\text{cold shell}}$ by the amount necessary to bring near agreement between the simulations and the measurements.)

IV. CONCLUSIONS

A series of direct-drive implosion experiments on low-pressure (3–15 atm) gas-filled CH, CD–CH, and CH targets with embedded Ti-doped CH layers has been performed on OMEGA. The target performance at stagnation and its dependence on beam smoothing and pulse shaping have been determined from the primary (D–D) and secondary (D–T) fusion neutron yields and spectral shapes, imaging of Ti-doped-shell x-ray emission, and imaged continuum x-ray spectroscopy.

The dependence of neutron yield on shell thickness and shell convergence ratio points to the shell's integrity as a dominant factor in target performance. The correlation of yield performance with pulse shape and the relative benefit of beam smoothing confirms this. The addition of beam smoothing is most beneficial to the shaped-pulse (least-stable) implosions. The performance of gas-filled CH targets is lower than empty CD–CH targets as a function of CR_{shell}. The gas-filled and empty-shell targets differ in that the former must suffer through the passage of a shock from shell to gas fill, to the center, and back to shell again as well as the deceleration-phase RT instability, while the latter do not (or to a minimal degree). The detrimental effects at the gas–shell interface lead to decreased target performance.

The neutron yields compared to 1D simulation predictions indicate that target performance is a function of beam smoothing, pulse shape, and initial target thickness. The thickest targets show the best performance and benefit the least from beam smoothing, while the thinnest targets imploded with the longer shaped pulses benefit the most from beam smoothing. The correlation of target performance with shell convergence ratio (CR_{shell}) suggests that shell integrity is important to target performance.

The effects of beam smoothing and pulse shaping on shell performance were also studied. First, the results from the secondary neutron yield confirm that the inside of the shell material at stagnation is both integral and has undergone little or no mixing. Secondly, x-ray images of Ti-doped inner shell regions at compression show that beam smoothing increases the shell integrity and compression despite the apparent lack of mixing. Lastly, beam smoothing strongly affects the outer shell region in all cases.

The target performance as a function of shell thickness and pulse shape depends on the separation of the shell inner surface from perturbations induced by single-beam laser nonuniformities. Targets imploded with slowly rising pulses have smaller in-flight shell thicknesses and higher RT growth rates than those imploded with rapidly rising ones. The slow falloff for the more stable (1 ns square pulse) implosions with shell convergence ratio is likely due to low *l*-mode perturbations caused by power imbalance. These would affect target performance in all cases but would become proportionally larger in magnitude for higher convergence ratios.

In summary, the dominant effect on target performance appears to be the shell stability. The outer (cold) shell region shows the most pronounced sensitivity to single-beam nonuniformities. The feedthrough of these perturbations to the inner shell and gas regions limits the target performance.

ACKNOWLEDGMENTS

The authors acknowledge the support of the OMEGA laser operations group, and the staff at the Laboratory for Laser Energetics of the University of Rochester. This work was supported by the U.S. Department of Energy Office of Inertial Confinement Fusion under Cooperative Agreement No. DE-FC03-92SF19460, the University of Rochester, and the New York State Energy Research and Development Authority. The support of DOE does not constitute an endorsement by DOE of the views expressed in this article.

[1] J. Nuckolls, L. Wood, A. Thiessen, and G. Zimmerman, Nature (London) **239**, 139 (1972).
[2] J. D. Lindl, *Inertial Confinement Fusion: The Quest for Ignition and Energy Gain Using Indirect Drive* (Springer-Verlag, New York, 1998).
[3] S. E. Bodner, D. G. Colombant, J. H. Gardner, R. H. Lehmberg, S. P. Obenschain, L. Phillips, A. J. Schmitt, J. D. Sethian, R. L. McCrory, W. Seka, C. P. Verdon, J. P. Knauer, B. B. Afeyan, and H. T. Powell, Phys. Plasmas **5**, 1901 (1998).
[4] J. D. Kilkenny, in *Current Trends in International Fusion Research*, edited by E. Panarella (Plenum, New York, 1997), p. 295.
[5] M. D. Rosen, Phys. Plasmas **3**, 1803 (1996).
[6] T. R. Boehly, D. L. Brown, R. S. Craxton, R. L. Keck, J. P. Knauer, J. H. Kelly, T. J. Kessler, S. A. Kumpan, S. J. Loucks, S. A. Letzring, F. J. Marshall, R. L. McCrory, S. F. B. Morse, W. Seka, J. M. Soures, and C. P. Verdon, Opt. Commun. **133**, 495 (1997).
[7] J. A. Delettrez, V. Yu. Glebov, F. J. Marshall, C. Stoeckl, B. Yaakobi, and D. D. Meyerhofer, Bull. Am. Phys. Soc. **44**, 192 (1999).
[8] J. M. Soures, R. L. McCrory, C. P. Verdon, A. Babushkin, R. E. Bahr, T. R. Boehly, R. Boni, D. K. Bradley, D. L. Brown, R. S. Craxton, J. A. Delettrez, W. R. Donaldson, R. Epstein, P. A. Jaanimagi, S. D. Jacobs, K. Kearney, R. L. Keck, J. H. Kelly, T. J. Kessler, R. L. Kremens, J. P. Knauer, S. A. Kumpan, S. A. Letzring, D. J. Lonobile, S. J. Loucks, L. D. Lund, F. J. Marshall, P. W. McKenty, D. D. Meyerhofer, S. F. B. Morse, A. Okishev, S. Papernov, G. Pien, W. Seka, R. Short, M. J. Shoup III, M. Skeldon, S. Skupsky, A. W. Schmid, D. J. Smith, S. Swales, M. Wittman, and B. Yaakobi, Phys. Plasmas **3**, 2108 (1996).
[9] D. K. Bradley, J. A. Delettrez, R. Epstein, R. P. J. Town, C. P. Verdon, B. Yaakobi, S. Regan, F. J. Marshall, T. R. Boehly, J. P. Knauer, D. D. Meyerhofer, V. A. Smalyuk, W. Seka, D. A. Haynes, Jr., M. Gunderson, G. Junkel, C. F. Hooper, Jr., P. M. Bell, T. J. Ognibene, and R. A. Lerche, Phys. Plasmas **5**, 1870 (1998).
[10] Laboratory for Laser Energetics LLE Review **78**, 82, See National Technical Service Document No. DOE/SF/19460-295 (NASA Ames Report

2020, 1999). Copies may be obtained from the National Technical Information Service, Springfield, VA, 22161.
[11]F. J. Marshall, J. A. Delettrez, V. Yu. Glebov, R. P. J. Town, B. Yaakobi, R. Kremens, and M. Cable, Phys. Plasmas **7**, 1006 (2000).
[12]B. Yaakobi, F. J. Marshall, and D. K. Bradley, Appl. Opt. **37**, 8074 (1998).
[13]B. Yaakobi and F. J. Marshall, J. Quant. Spectrosc. Radiat. Transf. **61**, 465 (1999).
[14]T. J. Kessler, Y. Lin, L. S. Iwan, W. P. Castle, C. Kellogg, J. Barone, E. Kowaluk, A. W. Schmid, K. L. Marshall, D. J. Smith, A. L. Rigatti, J. Warner, and A. R. Staley, in *Second Annual International Conference on Solid State Lasers for Application to Inertial Confinement Fusion*, edited by M. L. André (SPIE, Bellingham, WA, 1997), Vol. 3047, p. 272.
[15]S. Skupsky, R. W. Short, T. Kessler, R. S. Craxton, S. Letzring, and J. M. Soures, J. Appl. Phys. **66**, 3456 (1989).
[16]M. C. Richardson, P. W. McKenty, F. J. Marshall, C. P. Verdon, J. M. Soures, R. L. McCrory, O. Barnouin, R. S. Craxton, J. Delettrez, R. L. Hutchison, P. A. Jaanimagi, R. Keck, T. Kessler, H. Kim, S. A. Letzring, D. M. Roback, W. Seka, S. Skupsky, B. Yaakobi, S. M. Lane, and S. Prussin, in *Laser Interaction and Related Plasma Phenomena*, edited by H. Hora and G. H. Miley (Plenum, New York, 1986), Vol. 7, p. 421.
[17]D. D. Meyerhofer, P. W. McKenty, V. N. Goncharov, J. A. Delettrez, V. Yu. Glebov, F. J. Marshall, P. B. Radha, S. P. Regan, V. A. Smalyuk, J. M. Soures, C. Stoeckl, R. P. J. Town, B. Yaakobi, and R. D. Petrasso, Bull. Am. Phys. Soc. **44**, 193 (1999).
[18]J. P. Knauer, R. L. Kremens, M. A. Russotto, and S. Tudman, Rev. Sci. Instrum. **66**, 926 (1995).
[19]R. L. McCrory and C. P. Verdon, in *Inertial Confinement Fusion*, edited by A. Caruso and E. Sindoni (Editrice Compositori, Bologna, Italy, 1989).
[20]F. J. Marshall, J. A. Delettrez, R. Epstein, and B. Yaakobi, Phys. Rev. E **49**, 4381 (1994).